

## 1.5 $\mu\text{m}$ lasers with sub-10 mHz linewidth

D.G. Matei,<sup>1,\*</sup> T. Legero,<sup>1</sup> S. Häfner,<sup>1</sup> C. Grebing,<sup>1,†</sup> R. Weyrich,<sup>1</sup> W. Zhang,<sup>2</sup> L. Sonderhouse,<sup>2</sup> J.M. Robinson,<sup>2</sup> J. Ye,<sup>2</sup> F. Riehle,<sup>1</sup> and U. Sterr<sup>1</sup>

<sup>1</sup>*Physikalisch-Technische Bundesanstalt, Bundesallee 100, 38116 Braunschweig, Germany*

<sup>2</sup>*JILA, National Institute of Standards and Technology and University of Colorado, Department of Physics, 440 UCB, Boulder, Colorado 80309, USA*

We report on two ultrastable lasers each stabilized to independent silicon Fabry-Pérot cavities operated at 124 K. The fractional frequency instability of each laser is completely determined by the fundamental thermal Brownian noise of the mirror coatings with a flicker noise floor of  $4 \times 10^{-17}$  for integration times between 0.8 s and a few tens of seconds. We rigorously treat the notorious divergences encountered with the associated flicker frequency noise and derive methods to relate this noise to observable and practically relevant linewidths and coherence times. The individual laser linewidth obtained from the phase noise spectrum or the direct beat note between the two lasers can be as small as 5 mHz at 194 THz. From the measured phase evolution between the two laser fields we derive usable phase coherence times for different applications of 11 s to 55 s.

It is well known that frequency is the physical quantity that can be measured with by far the highest accuracy. “Never measure anything but frequency!” was the advice of Arthur Schawlow [1]. The high accuracy results from the fact that the phase of a purely periodic signal can be measured in the simplest case by counting the zero crossings of the signal within a given time or with even increased accuracy by a phase measurement that interpolates the signal between the zero crossings. Hence, the generation of truly phase coherent signals over long times is the key to precision measurements and enabling technologies. In the most advanced optical atomic clocks [2–5] pre-stabilized lasers serve as oscillators to interrogate ultranarrow optical transitions with linewidths of a few mHz. Oscillators with coherence times of tens to hundreds of seconds will allow for investigations of extremely small energy shifts in the clock transition, caused by sources such as interactions amongst atoms [6, 7]. Ultrastable oscillators beyond the state of the art will find useful applications in sub-mm very long baseline interferometry (VLBI) [8], atom interferometry and future atom-based gravitational wave detection [9–11], novel radar applications [12], the search for dark matter [13], and deep space navigation [14]. Consequently, large effort has been put into the development of extremely coherent sources based on highly stable optical Fabry-Pérot resonators [15–18]. Alternative schemes are currently being investigated using cavity-QED systems [17, 19] and spectral-hole burning in cryogenically cooled crystals [20].

Here we report on the coherence properties of two cavity-stabilized laser systems operating at a wavelength of 1542 nm. Our systems are based on well-isolated single-crystal silicon Fabry-Pérot resonators, temperature stabilized at 124 K. For a system that has well de-

signed locking electronics, the fractional frequency stability of the laser is given by the fractional stability of the optical length of the cavity. Fundamentally, the cavities’ length stability is limited by statistical Brownian noise of the mirror coatings, substrates, and spacer [21]. Due to the inherently low thermal noise of crystalline silicon, the cavities’ length fluctuations are dominated by the dielectric mirror coatings, despite their thickness of only a few tens of micrometers. The cryogenic cooling of the cavities further reduces the thermal noise and allows for a fractional length instability of the cavities of  $\Delta L/L \approx 10^{-17}$ .

Previously, with such a system (named Si1) we demonstrated a frequency instability of  $1 \times 10^{-16}$  [15]. We have now set up two systems (named Si2 and Si3) where we have reduced all additional noise sources [22] to a level well below the thermal noise limit.

In the following we describe briefly the set-up [23] and the analysis of the frequency stability and the phase noise. We subsequently derive methods to relate the dominant flicker frequency noise to observable and practically relevant linewidths and coherence times.

Each cavity consists of a plano-concave mirror pair employing high-reflectivity  $\text{Ta}_2\text{O}_5/\text{SiO}_2$  dielectric multilayers. The finesse of the  $\text{TEM}_{00}$  mode of each cavity is close to 500 000. The 212 mm long spacer and the mirror substrates are machined from single-crystal silicon [15]. The crystal orientation of the optically contacted substrates is aligned to that of the spacer. Both have the silicon  $\langle 111 \rangle$  axis oriented along the cavity axis.

The cavities are aligned vertically and are supported at three points near the midplane in order to minimize the impact of seismic and acoustic vibrations on their length stability. The anisotropic elasticity of silicon was used to minimize the vertical vibration sensitivity below  $10^{-12}/(\text{m s}^{-2})$  by adjusting the azimuthal angle between the cavity and its tripod support [22].

The cavities are placed in separate vacuum systems at a residual pressure below  $10^{-9}$  mbar. The cavity tem-

\* e-mail: dan.matei@ptb.de

† currently with TRUMPF Scientific Lasers GmbH + Co. KG, Feringastr. 10a, 85774 Unterföhring, Germany

perature is stabilized to 124 K where a zero crossing of the coefficient of thermal expansion of silicon occurs [15, 22]. Each system is mounted on separate optical tables, about 3 m apart. The systems have their own active vibration isolation platforms and are surrounded by individual acoustic and temperature insulation boxes. They strongly suppress individual and thus also common noise contributions to below the thermal noise level on timescales up to several minutes [22].

Commercial Er-doped distributed feedback (DFB) fiber lasers at 1542 nm ( $\nu_0 = 194.4$  THz) are frequency stabilized to the cavities using the Pound-Drever-Hall (PDH) method [24]. Fiber-coupled acousto-optic modulators (AOM) are used for the fast servo allowing locking bandwidths of around 150 kHz. Active residual amplitude modulation (RAM) cancellation [25] is employed to keep the corresponding fractional frequency fluctuations below the thermal noise level of the system [22].

To obtain the individual frequency instabilities of the Si2 and Si3 lasers, we compared them to a third ultra-stable laser based on a 48 cm long ultra low expansion glass (ULE) cavity at 698 nm [16]. The frequency gap between the 1.5  $\mu\text{m}$  Si2 system and the 698 nm ULE-cavity laser was bridged using a fiber-based optical frequency comb as a transfer oscillator [26, 27]. The comb introduces negligible noise that is below the thermal noise floor of the ULE cavity. Additional noise arising from the optical fibers connecting the lasers and the frequency comb is suppressed with active noise cancellation [28].

We measured the beat frequencies ‘Si2 – Si3’ and ‘Si2 – ULE’ using synchronized counters [29]. The third beat frequency ‘Si3 – ULE’ is calculated as their difference which is justified since our beat measurement system does not introduce appreciable additional noise.

We do not expect correlations between the ULE-cavity system, the optical frequency comb and the Si-systems, since they reside in three different rooms. Thus, the three difference frequencies allowed us to derive the three individual instabilities from a simple three-cornered hat analysis [30] (Fig. 1). The relative linear frequency drift between Si2 and Si3 of about 100  $\mu\text{Hz/s}$  (comparable with the figure reported in Ref. [31]) and between Si2 and the ULE-cavity laser of 15 mHz/s is removed.

The three-cornered hat results (Fig. 1) [33] indicate that for averaging times from 0.8 s up to 10 s the instability of each Si-based laser system is at the expected thermal noise flicker floor of  $\text{mod } \sigma_y = 4 \times 10^{-17}$ . This corresponds to a standard Allan deviation of about  $5 \times 10^{-17}$  [34]. For short averaging times the increase in the instability is due to residual vibration and acoustic noise. At long averaging times we see the effect of slow temperature fluctuations affecting the cavity length and of parasitic etalons in the optical setup.

A more complete characterization of the noise processes is given by the power spectral density (PSD) of the phase fluctuations. We have determined the phase of

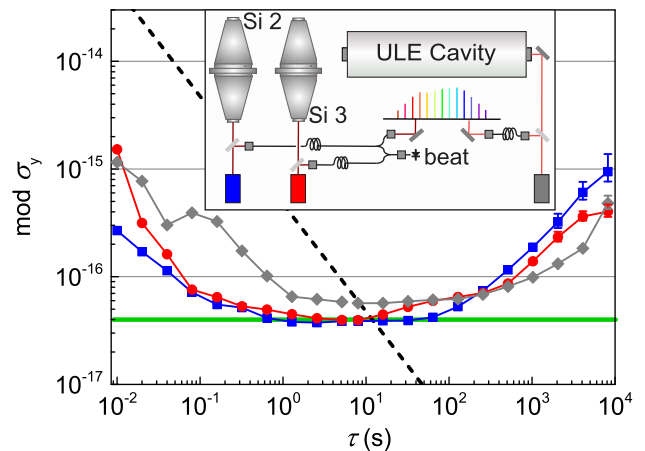


FIG. 1. Modified Allan deviation for Si2 (squares), Si3 (circles) and ULE-cavity laser (diamonds) derived from three-cornered hat estimations. We used a 3.4 h dataset for  $10 \text{ ms} \leq \tau \leq 4 \text{ s}$  and a 24.2 h dataset for  $8 \text{ s} \leq \tau \leq 8192 \text{ s}$ , recorded in the same day. The green line represents the expected thermal noise of the silicon cavities. The dashed line illustrates the instability where the rms phase fluctuations are 1 rad for a given  $\tau$  [32]. The intersections with the instability curves of the Si lasers result in coherence times of around 11 s. Linear frequency drifts in each dataset were subtracted. The inset shows a schematic of the measurement setup.

the beat signal from the measured in-phase and quadrature signal components. From more than 37 hours of phase data we determine the phase noise spectrum of a single laser down to Fourier frequencies of 0.1 mHz (Fig. 2), modeled as

$$S_{\phi}(f) = \nu_0^2 \sum_{k=-2}^0 h_k f^{k-2}. \quad (1)$$

From 1 mHz to 1 Hz the noise spectrum closely follows the thermal frequency flicker noise with  $h_{-1} = 1.7 \times 10^{-33}$ , in agreement with the expected thermal noise. From 1 Hz to 3 kHz the seismic and acoustic perturbations above the thermal noise lead to a number of narrow peaks. The base line of the spectrum can be approximated by white frequency noise with  $h_0 = 3.6 \times 10^{-33} \text{ Hz}^{-1}$  consistent with the increase of the instability at short averaging times (Fig. 1). Other possible sources such as photon shot-noise, RAM, laser power fluctuations are well below that level. At higher frequencies, the three broad peaks at 8 kHz, 60 kHz, and 150 kHz result from the servo loops for RAM regulation, fiber noise cancellation and PDH lock to the cavity, respectively. Below 1 mHz slow temperature fluctuations lead to a random walk frequency noise with  $h_{-2} = 4 \times 10^{-36} \text{ Hz}$ , corresponding to the Allan deviation values above 100 s.

In the following we use this data to derive values for laser linewidth and coherence time. Usually, linewidth and coherence time are derived from the autocorrelation function of the laser field with amplitude  $E_0$  and center

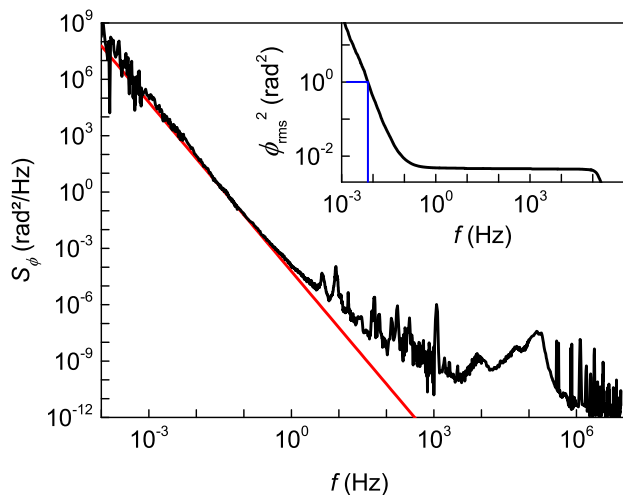


FIG. 2. PSD of phase fluctuations of a Si stabilized laser, obtained as one half of the PSD of the Si3 – Si2 beat. The red line shows the expected flicker frequency noise corresponding to the thermal noise at  $T = 124$  K. The inset shows the rms phase noise integrated down from 10 MHz. A value of  $1 \text{ rad}^2$  is obtained after integrating down to 6.8 mHz (blue markers) leading to a FWHM linewidth of 13.6 mHz.

frequency  $\nu_0$ ,

$$\begin{aligned} R_E(\tau) &= E_0^2 e^{i2\pi\nu_0\tau} e^{-1/2\langle(\phi(t+\tau)-\phi(t))^2\rangle}, \\ &= E_0^2 e^{i2\pi\nu_0\tau} e^{-2\int_0^\infty S_\phi(f) \sin^2(\pi f\tau) df}. \end{aligned} \quad (2)$$

Flicker frequency noise and random walk frequency noise are the dominant noise processes in our lasers. In this case the laser frequency  $\nu(t)$  is nonstationary and  $R_E(\tau)$  is divergent so that no unique coherence function can be assigned. This also leads to divergences in the general definition of the field spectrum  $S_E(\delta\nu)$  as the Fourier transform of the autocorrelation function  $R_E(\tau)$  (Eq. (2)) and thus no uniquely defined linewidth exists. Nevertheless we can derive linewidths that are closely related to the experimental observations.

If a spectrum is recorded for a measurement time  $T_0$  the linewidth is limited by the Fourier width proportional to  $1/T_0$  for short measuring times whereas for longer measurement times the nonstationary frequency fluctuations broaden the line. In such a case a practical linewidth can be defined by the minimum.

To elaborate this approach Bishof *et al.* [18] make the assumption that only Fourier components of the phase noise spectrum for frequencies  $f > 1/T_0$  contribute during the measurement time  $T_0$ . From our phase noise model (Eq. (1)) we obtain a minimal single laser linewidth of  $\Delta\nu_{\text{FWHM}} = 7$  mHz for  $T_0 = 170$  s [35].

Experimentally we obtain linewidths from a fast Fourier transform (FFT) of the beat between the two lasers, after the beat is mixed down to a carrier frequency suitable for data acquisition. We choose 200 s measurement time to allow for sufficiently high frequency resolu-

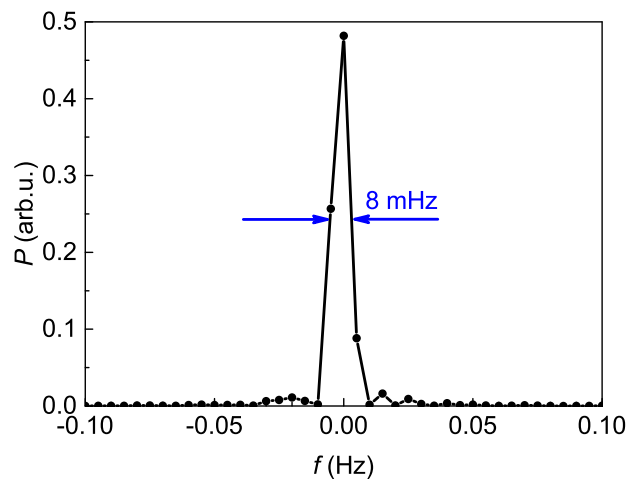


FIG. 3. FFT spectrum of the beat note between lasers Si2 and Si3 (Hanning window, frequency resolution 7.2 mHz).

tion while keeping the influence of slow frequency fluctuations small enough. Experimentally, in about 43% of the measurements [36] we obtain full-width-half-maximum (FWHM) linewidths of the beat signal between 7 mHz and 14 mHz (see Fig. 3), leading to individual linewidths  $\Delta\nu_{\text{FWHM}}$  between 5 mHz to 10 mHz, assuming that both lasers contribute equally to the linewidth. This standard approach of measuring the linewidth seems to give a reasonable agreement with the calculated minimal linewidth of 7 mHz according to Ref. [18].

To provide a linewidth estimate that includes all fluctuations of the flicker frequency noise, we averaged all FFT spectra obtained from the data set of 37 h after first aligning their centers of mass [36]. This results in an average linewidth for a single laser of about 13 mHz for a measurement time of 150 s. The difference between this longterm averaged value and the calculated minimal linewidth can be explained by the different ways the low-frequency cutoff is introduced. If a FFT spectrum analyzer is used the spectrum is centered at the average frequency during the measurement time  $T_0$  which corresponds to a subtraction of the linear phase evolution term. Thus significant quadratic terms still contribute to the phase excursion which correspond to noise at frequencies of approximately  $1/2T_0$  that is not included in the approximation of [18]. The narrower linewidths that we have observed (Fig. 3) are cases where the random quadratic term happened to be small.

Many applications are not directly sensitive to the FWHM linewidth but require sufficient spectral power in a narrow bandwidth  $\Delta\nu_P$ . This bandwidth can be estimated by integrating the phase noise from high-frequencies towards zero [37, 38]. The half bandwidth is obtained as the lower integration limit in

$$\int_{\Delta\nu_P/2}^{\infty} S_\phi(f) df = 1 \text{ rad}^2, \quad (3)$$

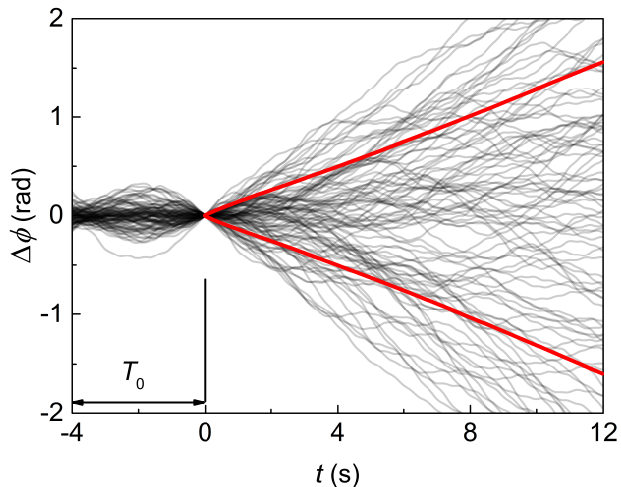


FIG. 4. The evolution of the phase difference between the two Si lasers. The first 4 s segment  $T_0$  is used to estimate the average frequency  $\bar{\nu}$  at  $t = 0$  s. For  $t = 0 - 12$  s, the phase deviation from the expected  $2\pi\bar{\nu}t$  is calculated. 100 consecutive curves are shown with thin gray lines. The red lines indicate the  $\pm\Delta\phi_{\text{rms}}$  range, evaluated statistically from 20 750 curves.

corresponding to the case when one third of the power is contained in the bandwidth  $\Delta\nu_P$  [38]. For this definition we find a value of  $\Delta\nu_P = 14$  mHz (see inset of Fig. 2).

For many applications it is important to provide effective coherence times of ultrastable oscillators. For this purpose, depending on the particular application, different methods must be employed to adequately consider the nonstationary frequency.

As an example more adequate for optical clocks we investigate a two-pulse Ramsey interrogation of atoms. There, an average frequency and frequency drift can be estimated from past measurements and considered in the current interrogation in order to keep the phase excursions  $\Delta\phi$  between the two pulses sufficiently small.

We simulate such a scenario using the phase evolution of the ‘Si2 – Si3’ beat recorded for 1 day. We cut this dataset into short samples and fit a linear phase to the first 4 s (i.e., observation interval  $T_0$ ) to determine the average frequency  $\bar{\nu}$ . The phase  $2\pi\bar{\nu}t$  is subtracted and the phase at  $t = 0$  is set to zero to obtain the phase deviation  $\Delta\phi$  for  $t \geq 0$ . Figure 4 shows 100 of these samples, which indicate a time-dependent broadening. The root-mean-square deviation  $\Delta\phi_{\text{rms}}(t)$  of the normally distributed phase deviation was calculated from 20 750 samples ( $\pm\Delta\phi_{\text{rms}}$  indicated by red lines). The coherence is certainly lost when the phase has acquired an uncertainty of  $\Delta\phi_{\text{rms}} \approx \pi$  (at  $t \approx 30$  s) but depending on the application, more restricting definitions of the coherence time are in use. In a more conservative way we define the coherence time as a duration in which  $\Delta\phi_{\text{rms}}$  has increased to 1 rad (i.e.,  $\sqrt{2}$  rad for the phase difference between the two independent lasers shown in Fig.

4). In agreement with the value estimated from the Allan deviation (Fig. 1) [32], this leads to a coherence time of 11 s. This is equivalent to saying that after 11 s in more than 99% of all cases the actual phase excursions remain below  $\pm\pi \approx 3\phi_{\text{rms}}$ , which ensures unambiguous phase tracing. We find that this value of 11 s represents a broad maximum in the coherence time when the Ramsey interrogation time varies between 4 s and 20 s [32].

Besides situations where the future phase must be predicted there are many applications where the average frequency can be determined in retrospect from the measurement itself. Typical examples are spectral analysis, when the spectrum is centered, or the Rabi interrogation of atoms by single pulses, where the observed excitation provides the information of the average frequency during the measurement time. Analysis of our measured phase data shows that in this case an rms phase deviation of  $\Delta\phi_{\text{rms}} = 1$  rad occurs at measurement intervals of about 55 s [32].

In conclusion, we have demonstrated the operation of two cryogenic optical silicon cavities at the thermal noise limit of  $\text{mod } \sigma_y = 4 \times 10^{-17}$ . The light stabilized on these cavities is highly coherent, with a coherence time of 11 s to 55 s. As seen from the spectral analysis, the linewidth and implicitly the coherence time are mostly determined by the thermal noise level. With this kind of laser sources we are now entering the regime where the frequency stability of the interrogation laser is on a par with the quantum projection noise limit of today’s most stable optical clocks (e.g. [39, 40]).

Optimizations of the current setup would hardly bring a longer coherence time since we are nearing a fundamental limit. The only way of further improving the current performance is to decrease the thermal noise even further. One approach is to decrease the temperature, thus reducing the thermal motion in the system. For an operating temperature of 4 K the expected thermal noise would be  $8 \times 10^{-18}$  in the modified Allan deviation. A comparable noise figure would be achieved by employing AlGaAs-based crystalline coatings, which offer a higher mechanical  $Q$  factor and thus a lower thermal-induced noise [41, 42]. If both methods are implemented, the thermal noise would be reduced to the lower half of the  $10^{-18}$  range, roughly an order of magnitude lower than the present level. To ensure that this improvement leads to an increased coherence time it is necessary to reduce the longterm instability for averaging times above 10 s (see intersection of dashed line with the thermal noise level in Fig. 1) while the present short-term instability seems to be sufficiently small.

Our rigorous analysis of linewidth and coherence time will be tremendously important when we start using this state-of-the-art laser e.g. for investigations of classical and/or quantum correlated atoms [43]. Achieving enhanced stability from quantum correlation (such as spin squeezing) will need a local oscillator that does not intro-



duce excessive phase noise which can easily remove the benefit of correlation [44].

This silicon cavity work is supported and developed jointly by the Centre for Quantum Engineering and Space-Time Research (QUEST), Physikalisch-Technische Bundesanstalt (PTB), the JILA Physics Frontier Center (NSF), the National Institute of Standards and Technology (NIST). This project has received funding under 15SIB03 OC18 from the EMPIR programme co-financed by the Participating States and from the European Union's Horizon 2020 research and innovation programme. We also acknowledge support by the European Metrology Research Programme (EMRP) under QESOCAS. The EMRP is jointly funded by the EMRP participating countries within EURAMET, and the European Union. We thank U. Kuetsgens and D. Schulze for x-ray orientation of the spacer and mirrors, and E. Oelker for comments about the manuscript. J. Ye thanks the Alexander von Humboldt Foundation for support. L. Sonderhouse is supported by the National Defense Science and Engineering Graduate (NDSEG) fellowship.

- 
- [1] T. W. Hänsch, *Rev. Mod. Phys.* **78**, 1297 (2006).
- [2] A. D. Ludlow, M. M. Boyd, J. Ye, E. Peik, and P. O. Schmidt, *Rev. Mod. Phys.* **87**, 637 (2015).
- [3] T. L. Nicholson, S. L. Campbell, R. B. Hutson, G. E. Marti, B. J. Bloom, R. L. McNally, W. Zhang, M. D. Barrett, M. S. Safronova, G. F. Strouse, W. L. Tew, and J. Ye, *Nature Com.* **6**, 6896 (2015).
- [4] I. Ushijima, M. Takamoto, M. Das, T. Ohkubo, and H. Katori, *Nature Photonics* **9**, 185 (2015).
- [5] N. Huntemann, C. Sanner, B. Lipphardt, C. Tamm, and E. Peik, *Phys. Rev. Lett.* **116**, 063001 (2016).
- [6] A. M. Rey, A. V. Gorshkov, C. V. Kraus, M. J. Martin, M. Bishof, M. D. Swallows, X. Zhang, C. Benko, J. Ye, N. D. Lemke, and A. D. Ludlow, *Annals of Physics* **340**, 311 (2014).
- [7] M. J. Martin, M. Bishof, M. D. Swallows, X. Zhang, C. Benko, J. von Stecher, A. V. Gorshkov, A. M. Rey, and J. Ye, *Science* **341**, 632 (2013).
- [8] S. Doeleman, T. Mai, A. E. E. Rogers, J. G. Hartnett, M. E. Tobar, and N. Nand, *Publ. Astron. Soc. Pac.* **123**, 582 (2011).
- [9] J. M. Hogan and M. A. Kasevich, *Phys. Rev. A* **94**, 033632 (2016).
- [10] S. Kolkowitz, I. Pikovski, N. Langellier, M. D. Lukin, R. L. Walsworth, and J. Ye, *Phys. Rev. D* **94**, 124043 (2016).
- [11] B. Canuel, S. Pelisson, L. Amand, A. Bertoldi, E. Cormier, B. Fang, S. Gaffet, R. Geiger, J. Harms, D. Holleville, A. Landragin, G. Lefèvre, J. Lhermite, N. Mielec, M. Prevedelli, I. Riou, and P. Bouyer, *Proc. SPIE* **9900**, 990008 (2016).
- [12] P. Ghelfi, F. Laghezza, F. Scotti, G. Serafino, A. Capria, S. Pinna, D. Onori, C. Porzi, M. Scaffardi, A. Malacarne, V. Vercesi, E. Lazzeri, F. Berizzi, and A. Bogoni, *Nature* **507**, 341 (2014).
- [13] A. Derevianko and M. Pospelov, *Nature Physics* **10**, 933 (2014).
- [14] S. Grop, P. Y. Bourgeois, N. Bazin, Y. Kersalé, E. Rubiola, C. Langham, M. Oxborrow, D. Clapton, S. Walker, J. De Vicente, and V. Giordano, *Rev. Sci. Instrum.* **81**, 025102 (2010).
- [15] T. Kessler, C. Hagemann, C. Grebing, T. Legero, U. Sterr, F. Riehle, M. J. Martin, L. Chen, and J. Ye, *Nature Photonics* **6**, 687 (2012).
- [16] S. Häfner, S. Falke, C. Grebing, S. Vogt, T. Legero, M. Merimaa, C. Lisdat, and U. Sterr, *Opt. Lett.* **40**, 2112 (2015).
- [17] M. A. Norcia and J. K. Thompson, *Phys. Rev. X* **6**, 011025 (2016).
- [18] M. Bishof, X. Zhang, M. J. Martin, and J. Ye, *Phys. Rev. Lett.* **111**, 093604 (2013).
- [19] B. T. R. Christensen, M. R. Henriksen, S. A. Schäffer, P. G. Westergaard, D. Trier, J. Ye, M. J. Holland, and J. W. Thomsen, *Phys. Rev. A* **92**, 053820 (2015).
- [20] S. Cook, T. Rosenband, and D. R. Leibbrandt, *Phys. Rev. Lett.* **114**, 253902 (2015).
- [21] K. Numata, A. Kemery, and J. Camp, *Phys. Rev. Lett.* **93**, 250602 (2004).
- [22] D. G. Matei, T. Legero, C. Grebing, S. Häfner, C. Lisdat, R. Weyrich, W. Zhang, L. Sonderhouse, J. M. Robinson, F. Riehle, J. Ye, and U. Sterr, *J. Phys.: Conf. Ser.* **723**, 012031 (2016).
- [23] Supplemental Material, ‘Set-up: reduction of technical noise’.
- [24] R. W. P. Drever, J. L. Hall, F. V. Kowalski, J. Hough, G. M. Ford, A. J. Munley, and H. Ward, *Appl. Phys. B* **31**, 97 (1983).
- [25] W. Zhang, M. J. Martin, C. Benko, J. L. Hall, J. Ye, C. Hagemann, T. Legero, U. Sterr, F. Riehle, G. D. Cole, and M. Aspelmeyer, *Opt. Lett.* **39**, 1980 (2014).
- [26] H. R. Telle, B. Lipphardt, and J. Stenger, *Appl. Phys. B* **74**, 1 (2002).
- [27] J. Stenger, H. Schnatz, C. Tamm, and H. R. Telle, *Phys. Rev. Lett.* **88**, 073601 (2002).
- [28] L.-S. Ma, P. Jungner, J. Ye, and J. L. Hall, *Opt. Lett.* **19**, 1777 (1994).
- [29] G. Kramer and W. Klische, in *Proceedings of the 18th European Frequency and Time Forum, Guildford, UK* (IET, London, UK, 2004) pp. 595–602.
- [30] J. E. Gray and D. W. Allan, in *Proceedings of the 28th Annual Symposium on Frequency Control, 29-31 May 1974, Atlantic City, New Jersey, New Jersey* (Electronic Industries Association, 2001 Eye Street, N.W., Washington, D.C. 20006, 1974) pp. 243–246.
- [31] C. Hagemann, C. Grebing, C. Lisdat, S. Falke, T. Legero, U. Sterr, F. Riehle, M. J. Martin, and J. Ye, *Opt. Lett.* **39**, 5102 (2014).
- [32] Supplemental Material, ‘Coherence time’.
- [33] Supplemental Material, ‘Allan deviation’.
- [34] S. T. Dawkins, J. J. McFerran, and A. N. Luiten, *IEEE Trans. Ultrason. Ferroelectr. Freq. Control* **54**, 918 (2007).
- [35] Supplemental Material, ‘Spectral width calculations’.
- [36] Supplemental Material, ‘FFT statistics’.
- [37] F. L. Walls and A. E. Wainwright, *IEEE Trans. Instrum. Meas.* **24**, 15 (1975).
- [38] J. L. Hall and M. Zhu, in *Laser Manipulation of Atoms and Ions*, Proceedings Internat. School of Physics “Enrico Fermi”, Vol. Course CXVIII (North Holland–

- Elsevier, Amsterdam, 1992) pp. 671–702.
- [39] M. Schioppo, R. C. Brown, W. F. McGrew, N. Hinkley, R. J. Fasano, K. Beloy, T. H. Yoon, G. Milani, D. Nicolodi, J. A. Sherman, N. B. Phillips, C. W. Oates, and A. D. Ludlow, *Nature Photonics* **11**, 48 (2017).
- [40] S. L. Campbell, R. B. Hutson, G. E. Marti, A. Goban, N. D. Oppong, R. L. McNally, L. Sonderhouse, J. M. Robinson, W. Zhang, B. J. Bloom, and J. Ye, “A Fermi-degenerate three-dimensional optical lattice clock,” arXiv:1702.01210 [physics.atom-ph] (2017), arXiv:1702.01210.
- [41] G. D. Cole, W. Zhang, M. J. Martin, J. Ye, and M. Aspelmeyer, *Nature Photonics* **7**, 644 (2013).
- [42] G. D. Cole, W. Zhang, B. J. Bjork, D. Follman, P. Heu, C. Deutsch, L. Sonderhouse, J. Robinson, C. Franz, A. Alexandrovski, M. Notcutt, O. H. Heckl, J. Ye, and M. Aspelmeyer, *Optica* **3**, 647 (2016).
- [43] E. Paladino, Y. M. Galperin, G. Falci, and B. L. Altshuler, *Rev. Mod. Phys.* **86**, 361 (2014).
- [44] E. M. Kessler, P. Kómár, M. Bishof, L. Jiang, A. S. Sørensen, J. Ye, and M. D. Lukin, *Phys. Rev. Lett.* **112**, 190403 (2014).

## Supplemental Material for 1.5 $\mu\text{m}$ lasers with sub-10 mHz linewidth

### SET-UP: REDUCTION OF TECHNICAL NOISE

The fractional frequency stability of the laser is directly related to the fractional stability of the optical length of the cavity. We therefore ensured that the external factors are reduced below the level given by the statistical Brownian noise. We address in the following the influence of temperature, laser power fluctuations, mechanical vibrations, and residual gas pressure fluctuations.

As temperature changes induce length fluctuations through thermal expansion, the operating point of the cryostat is chosen such that the cavity temperature precisely matches the zero-crossing point of the coefficient of thermal expansion (CTE) [S1], thus reducing the impact of temperature fluctuations. These are further reduced by enclosing the cavity in two concentric thermal shields, with the outer one being temperature-stabilized using a flow of nitrogen gas and the inner one serving as a buffer. Care has been taken also to reduce the blackbody radiation of the environment reaching the cavity, by using windows that block most of it and by limiting the solid angle through which the radiation can enter. The coefficients for the heat transfer from the room temperature environment to the inner shield and to the cavity were measured for Si3 to be 8(2)  $\mu\text{W}/\text{K}$  and 6(2)  $\mu\text{W}/\text{K}$ , respectively. For the same system, the time constants for the heat flow between cavity and inner shield and inner shield and active shield are 1.3 days and 6.5 days, respectively. The temperature fluctuations of the cavity are thus reduced to below 1 nK for averaging times of a few seconds and affect the length stability only for times of thousands of seconds or longer [S2].

Fluctuations of the intracavity laser power lead to path length fluctuations due to heating caused by the absorbed power. We measured a value of  $1.7(2) \times 10^{-15} (\mu\text{W})^{-1}$  for both cavities for the proportionality coefficient between fractional frequency and transmitted power fluctuations. The coefficient is small because the cavity is operated

near the zero CTE point of the mirror substrates and due to their high thermal conductivity, and thus no active control of the intensity is needed.

Vibrations transmitted to the cavity can change its dimensions, leading to frequency instability. Thus we minimized the sensitivity to accelerations in all directions by employing a stiff holding frame. In addition, the sensitivity to vertical accelerations ( $k_z$ ) was experimentally minimized by changing the angle between the three point support and the crystalline axis [S2]. The acceleration sensitivities are summarized in Table SI.

TABLE SI. Acceleration sensitivities for the Si2 and Si3 cavities.

System	sensitivities ( $10^{-12} / \text{ms}^{-2}$ )		
	$k_x$	$k_y$	$k_z$
Si2	2.5(12)	0.7(6)	0.4(5)
Si3	8.6(7)	4.0(2)	0.8(5)

Combined with the measured seismic vibrational spectrum, this ensures that the vibration-induced frequency noise is below the thermal-noise limit for averaging times above 100 ms [S2].

Fluctuations in the residual gas pressure present in ion pumps [S3] also induce frequency instabilities by changing the refractive index of the residual gas between the mirrors and thus altering the optical length. Using ultra-high-vacuum compatible materials and keeping the ion pumps always in the low pressure range, we achieve a stable base pressure of  $10^{-9}$  mbar. From the observed pressure fluctuations we estimate that corresponding frequency fluctuations are below  $4 \times 10^{-17}$  for averaging times shorter than a few thousand seconds.

## ALLAN DEVIATION

The modified Allan deviation (mod  $\sigma_y$ ) is used to characterize the frequency stability. It reduces the impact of high frequency phase noise on the stability values at longer averaging times, as our beat signals contain phase noise at high frequencies that arises from the frequency comb [S4] and from laser noise at frequencies above the bandwidth of the PDH locks. The modified Allan deviation also enables to distinguish different types of noise, typically indistinguishable in the Allan deviation [S5, S6].

The modified Allan deviation requires frequency counters that temporally average the frequency fluctuations with a triangular weighting function (so-called  $\Lambda$ -counters [S7, S8]). As our counters [S9] only approximate the  $\Lambda$ -sensitivity from 1 ms measurements with constant weighting function ( $\Pi$ -counter), we additionally band-pass filter the signals with bandwidths of about 1 kHz to better approximate the correct sensitivity function.

## SPECTRAL WIDTH CALCULATIONS

The Wiener-Khintchine theorem relates the field spectrum  $S_E$  to the Fourier transform of the field autocorrelation function

$$R_E(\tau) = \langle E(t+\tau)E^*(t) \rangle. \quad (\text{S4})$$

For a field  $E(t) = E_0 e^{2\pi i \nu_0 t} e^{i\phi(t)}$  with average frequency  $\nu_0$  and random phase  $\phi(t)$  this autocorrelation function can be expressed as

$$R_E(\tau) = E_0^2 e^{2\pi i \nu_0 \tau} \exp\left(-\frac{1}{2} \Delta\phi_{\text{rms}}^2(\tau)\right) \quad (\text{S5})$$

where we have used the root-mean-square (rms) phase increment

$$\Delta\phi_{\text{rms}}^2(\tau) = \langle (\phi(t+\tau) - \phi(t))^2 \rangle. \quad (\text{S6})$$

The phase increment can be calculated with a sensitivity function

$$h^{(\tau)}(t) = \delta(t-\tau) - \delta(t) \quad (\text{S7})$$

as

$$\phi(t+\tau) - \phi(t) = \int \phi(t+t')h(t')dt', \quad (\text{S8})$$

using the Dirac delta function  $\delta(t)$ . With the help of Parseval's theorem, the rms value of this convolution can be expressed through the power spectral density of phase fluctuations  $S_\phi(f)$  as

$$\Delta\phi_{\text{rms}}^2(\tau) = \int_0^\infty S_\phi(f) |H(f)|^2 df \quad (\text{S9})$$

$$= 4 \int_0^\infty S_\phi(f) \sin^2(\pi f \tau) df \quad (\text{S10})$$

where we use the Fourier transform of the sensitivity function  $h(t)$

$$H(f) = \int_0^{T_0} h(t) \exp(2\pi i f t) dt. \quad (\text{S11})$$

With the power spectral density of frequency fluctuations  $S_\nu(f) = f^2 S_\phi(f)$  the corresponding autocorrelation function reads

$$R_E(\tau) = E_0^2 e^{2\pi i \nu_0 \tau} \exp\left(-2 \int_0^\infty S_\nu(f) \frac{\sin^2(\pi f \tau)}{f^2} df\right). \quad (\text{S12})$$

However, for frequency noise processes  $S_\nu \propto f^k$  that are diverging towards zero frequency with  $k \leq -1$ , this autocorrelation function is diverging. This is due to the fact that the phase difference, expressed by the average frequency  $\bar{\nu}_\tau(t)$  in the interval  $[t, t+\tau]$

$$\Delta\phi(t) = \phi(t+\tau) - \phi(t) \quad (\text{S13})$$

$$= 2\pi\tau\bar{\nu}_\tau(t) \quad (\text{S14})$$

is nonstationary, so the expectation value needed to define the autocorrelation function  $R_E$  does not exist.

A similar problem appears when trying to use the classical frequency variance  $\langle \bar{\nu}(t)^2 \rangle$  to describe the stability of oscillators in time domain [S10]. There the Allan variance  $\sigma_\nu^2$  is now widely used instead to describe the stability of such sources, which circumvents the divergence of the classical variance by taking the variance between successive average frequencies:

$$\sigma_\nu^2(\tau) = \frac{1}{2} \langle (\bar{\nu}_\tau(t+\tau) - \bar{\nu}_\tau(t))^2 \rangle. \quad (\text{S15})$$

## Low-frequency cutoff methods

As only finite observation times  $T_0$  are used in any real experiment, it is common to avoid the divergence by introducing low-frequency cutoffs  $f_{\text{co}}$  in Eq. (S12). In the work of Stephan *et al.* [S11] a cutoff at  $f_{\text{co}} = 1/\tau$  is introduced. For pure flicker noise  $S_\nu = h_{-1} f^{-1}$  this approach leads to a Gaussian line profile and an effective FWHM linewidth  $\Delta\nu = 0.3537\nu_0 \sqrt{h_{-1}}$  independent of observation time.

Bishop *et al.* [S12] introduce a cutoff at  $f_{\text{co}} = 1/T_0$ , which leads to a linewidth that depends on the observation time  $T_0$ , and its minimum is used as the effective linewidth. To include also the Fourier width due to the limited observation time, windowing functions  $w(t)$  are employed in the finite-length Fourier transform [S13], leading to a spectrum of

$$S_E(f) = \int_0^\infty W(\tau) R_E(\tau) \cos(2\pi f \tau) d\tau. \quad (\text{S16})$$

Here the weighting function for the autocorrelation function  $W(\tau)$  is the convolution of the initial weighting function with itself  $W(\tau) = (w * w)(\tau)$ . E.g. in the case of a

rectangular window function of duration  $T_0$  it is

$$W(\tau) = (1 - |\tau|/T_0). \quad (\text{S17})$$

### Practical spectral measurements

The above methods do not directly correspond to practically employed spectral measurements. One widely used method to measure an effective linewidth is the spectral analysis of the beat signal between two similar oscillators during a limited measurement duration  $T_0$  using spectrum analyzer [S14], often based on a Fast Fourier Transform (FFT) of the signal. Here naturally only the width is recorded, while the average frequency of the beat is manually tracked to keep the signal within the observation bandwidth, which compensates for the nonstationary frequency of flicker noise. E.g. for a spectral measurement of duration  $T_0$ , the average frequency can be determined from the spectrum itself as the central frequency of the observed spectral feature.

Mathematically, this means that no longer the complete phase evolution  $\phi(t)$  is analyzed over infinite durations. Instead the expectation value of finite duration spectra from  $\phi^{(\text{cor})}(t)$  are considered, where the phase  $\phi^{(\text{av})}(t)$  due to the average frequency  $\nu^{\text{av}}$  is subtracted from each individual spectrum. Thus the variance of the phase increments in Eq. (S6) is not taken from the real laser phase but for the phase increments corrected by an average phase increment  $2\pi\nu^{(\text{av})}(t_2 - t_1)$  during the observation time with an average frequency  $\nu^{(\text{av})}$ .

Steck [S15] uses a weighted averaging depending on  $\tau$  and  $T_0$  to obtain a FWHM as function of  $T_0$ . Its minimum for flicker noise  $S_\nu(f) = h_{-1}/f$  is  $0.5\nu_0\sqrt{h_{-1}}$  at  $T_0 = 14\nu_0/\sqrt{h_{-1}}$ .

It should be noted that, due to this subtraction, the corrected phase increment in the observation interval in general is no longer invariant to time translation, but now depends on the two times:  $\Delta\phi(t_1, t_2)$ . The finite-length spectrum (periodogram) with window function  $w(t)$  is given as absolute squared Fourier transform of the signal:

$$\begin{aligned} S_E(f) &= |\mathcal{F}_E(f)|^2 \\ &= \int_0^{T_0} \int_0^{T_0} w(t_1)w(t_2)e^{-\frac{1}{2}i\Delta\phi^2(t_1, t_2)} \\ &\quad \cdot \cos(2\pi f(t_2 - t_1))dt_1dt_2. \end{aligned} \quad (\text{S18})$$

In the simplest way, the average frequency can be calculated from the phase increment during the interval  $[t, t + T_0]$ :

$$\phi^{(\text{av})} = 2\pi\tau\bar{\nu}(t) = \phi(t + T_0) - \phi(t). \quad (\text{S19})$$

The sensitivity function that corresponds to this interpolation by the average frequency is

$$h^{(\text{int})}(t_1, t_2) = (t_2 - t_1)/T_0 (\delta(t - T_0) - \delta(t)), \quad (\text{S20})$$

with the corresponding Fourier transforms

$$H^{(\tau)}(t_1, t_2, f) = e^{2\pi ift_2} - e^{2\pi ift_1}, \quad (\text{S21})$$

$$H^{(\text{int})}(t_1, t_2, f) = (t_2 - t_1)/T_0 (e^{2\pi ifT_0} - 1), \quad (\text{S22})$$

$$H^{(\text{diff})}(t_1, t_2, f) = H^{(\tau)}(t_1, t_2, f) - H^{(\text{int})}(t_1, t_2, f) \quad (\text{S23})$$

The rms phase deviation  $\Delta\phi_{\text{rms}}(t_1, t_2)$  is thus expressed with the help of Parseval's theorem as:

$$\Delta\phi_{\text{rms}}^2(t_1, t_2) = \int_0^\infty S_\phi(f) \left| H^{(\text{diff})}(t_1, t_2, f) \right|^2 df. \quad (\text{S24})$$

An example of  $\Delta\phi_{\text{rms}}(t_1, t_2)$  using a least-squares fit of the laser phase with  $T_0 = 60$  s is shown in Fig. S5. The figure indicates clearly that the phase deviation does not simply depend on the difference  $t_1 - t_2$ . The chart provides the full information of rms phase deviations for different measurement scenarios. The lower edge of the diagram, showing  $\Delta\phi_{\text{rms}}(0, t_2)$ , applies to Rabi interrogation and will be discussed below in connection to the experimental data shown in Fig. S11. The data relevant for Ramsey interrogation are visible in the stripe ( $t_1 = 60$  s,  $t_2 > 60$  s). The diagram and the underlying calculations provide also the relevant information if there is a gap between the initial observation interval and the subsequent prediction.

With the rms phase deviation  $\Delta\phi_{\text{rms}}(t_1, t_2)$  and a window function  $w(t)$  one calculates the field autocorrelation for  $\tau > 0$

$$R_E(\tau) = E_0^2 \int_0^{T_0 - \tau} w(t)w(t + \tau) e^{-\frac{1}{2}\Delta\phi_{\text{rms}}^2(t, t + \tau)} dt \quad (\text{S25})$$

and the spectrum according to Eq. (S18).

A better approximation to the average frequency is a least-squares fit to the laser phase, weighted by the window function  $w(t)$  of the FFT. Without loss of generality we consider the interval  $[0, T_0]$ . For the fit we use a sum of orthogonal polynomials  $\Pi_k(t)$  over the interval  $[0, T_0]$  with weight  $w(t)$ . For constant weight  $w = 1$  these are the shifted Legendre polynomials. Then in the least-squares sense the phase is approximated by

$$\phi^{\text{fit}}(t) = \sum_{k=0}^N c_k \Pi_k(t), \quad (\text{S26})$$

with coefficients

$$c_k = \int_0^{T_0} w(t)\Pi_k(t)\phi(t)dt. \quad (\text{S27})$$

Thus these coefficients can be expressed as convolution between the phase  $\phi(t)$  and a kernel  $w(t)\Pi_k(t)$ , and the variance of the corrected phase can be expressed with the help of Parseval's theorem through the product of  $S_\phi$  and the square of the absolute value of the Fourier transform  $\mathcal{F}(w(t)\Pi_k(t))$ .



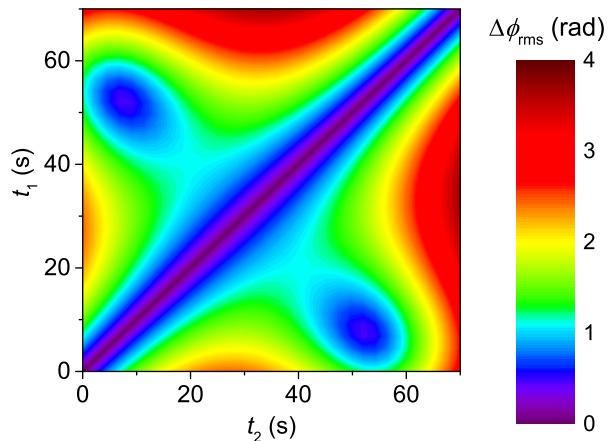


FIG. S5. Phase deviation  $\Delta\phi_{\text{rms}}(t_1, t_2)$  for the experimentally observed spectrum of frequency fluctuations, a duration of the observation interval  $T_0 = 60$  s and a fit with rectangular weighting function.

The rectangular (constant) weighting window and the Hanning window [S13]

$$w(t) = 1 - \cos(2\pi t/T_0) \quad (\text{S28})$$

are widely used in FFT spectral analysis. For both window functions we have calculated the phase variance (Fig. S5) and the linewidth as function of the measurement interval length  $T_0$  (Fig. S6 (filled symbols) and Fig. S7). If only the linear phase is fitted ( $N = 1$ ), we expect to obtain the linewidth of the averaged spectra. If the fit also includes a quadratic term ( $N = 2$ ), we expect to find the minimum observed linewidth, as during these measurements the actual frequency drift (i.e. the quadratic phase) was close to zero.

### FFT statistics

For a complete characterization of the linewidth measurements with FFT we used the 37 h phase record employed for calculating the phase noise spectrum. The data was broken up in adjacent equal-length segments and a FFT spectrum was obtained for each of them. The spectra were aligned on the frequency axis with their centers of mass at 0 Hz. For a finer alignment, the resolution bandwidth of the FFT was increased artificially by zero-padding the segments up to eight times their length. For each frequency the mean value from all spectra was calculated, resulting in an averaged spectrum as displayed in Fig. S8. When varying the length of the segments we obtain the data shown in Fig. S6 with open symbols. It results that the optimum interval length for obtaining a minimal linewidth lies between 120 s and 150 s.

Since the individual FFT spectra usually have irregular shapes to which no analytic peak function can be

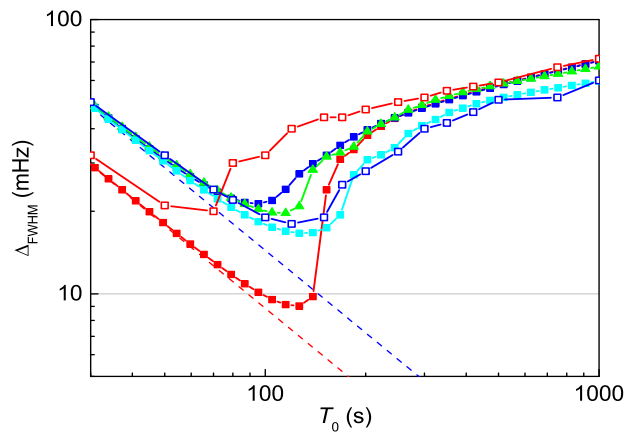


FIG. S6. FWHM beat linewidth  $\Delta_{\text{FWHM}}$  as a function of observation time  $T_0$ . Filled symbols: Calculations using the modeled phase noise spectrum and different methods to deal with the low-frequency divergence: with a cutoff at  $f = 1/T_0$  [S12] and rectangular window (red squares) or Hanning window (blue squares), with subtraction of phase frequency from weighted linear fit and Hanning window (green triangles) and with weighted quadratic fit and Hanning window (cyan squares). Open symbols: Linewidths obtained by averaging FFT spectra obtained with different window functions: rectangular (red squares) and Hanning (blue squares). The dashed lines indicate the respective Fourier limits of the rectangular (red) or Hanning window (blue).

assigned, we use an empirical approach in estimating their linewidths. First the maximum value was determined. Then the maximum was approached from both ends of the spectrum until the half-value was encountered. The difference between the two frequency values was then taken as the FWHM value. Using the data from Fig. S8 we obtain a linewidth of 19 mHz (for a Hanning window) of the beat, which results in a single-laser average linewidth of about 13 mHz. We also calculate the

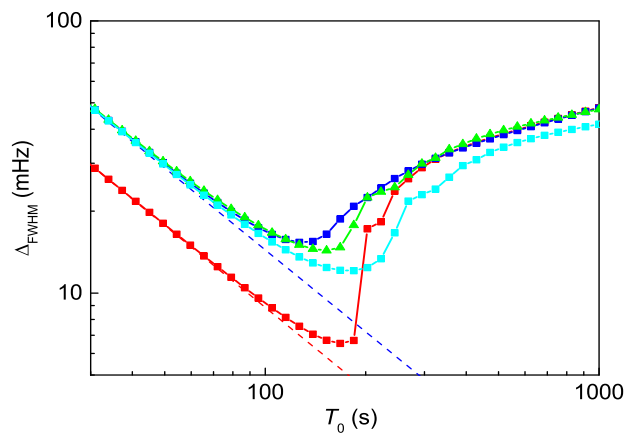


FIG. S7. Single laser FWHM linewidth  $\Delta_{\text{FWHM}}$  as a function of observation time  $T_0$  calculated from the modeled phase noise spectrum. For plot legend see caption of Fig. S6.

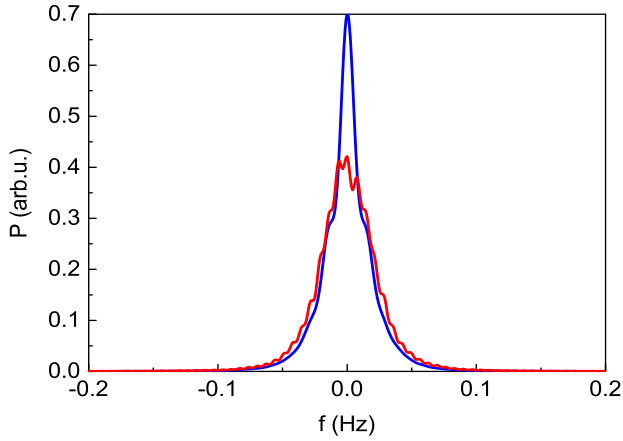


FIG. S8. Averaged FFT spectrum of the beat of the two lasers obtained from a phase measurement of 37 h by averaging all spectra obtained from 150 s intervals with a rectangular window (red line) and Hanning window (blue line). The increased frequency resolution results from zero-padding the data before the FFT calculation.

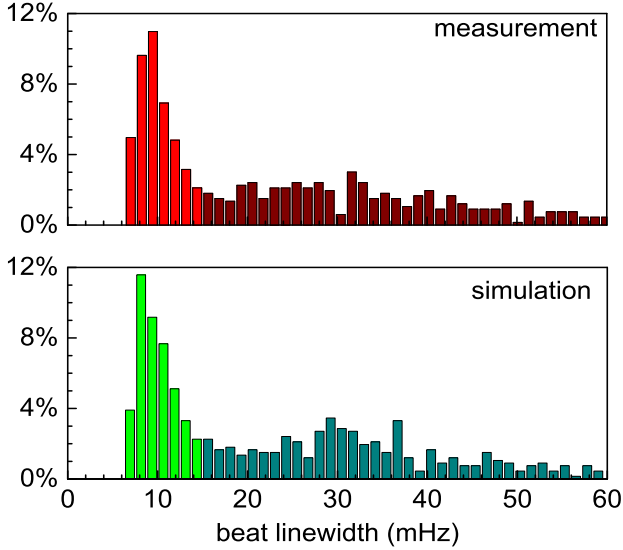


FIG. S9. Histogram of spectral linewidths for measured beat data (upper graph) and simulated flicker frequency noise (lower graph) corresponding to 200 s segments obtained from a 37 h record.

distribution of linewidths over the time span of 37 h. The result is shown in the upper graph from Fig. S9 for an interval of 200 s. This corresponds to the measurement with a FFT analyzer shown in the main text. The highlighted part represents the beat linewidths below 14 mHz which amounts to 43% of all measurements. For comparison, the same analysis for a simulated pure flicker frequency noise is shown in the lower graph. The similarity of the two histograms confirms once again that in this time range the behavior of the lasers is essentially described by a flicker frequency noise and that the broad

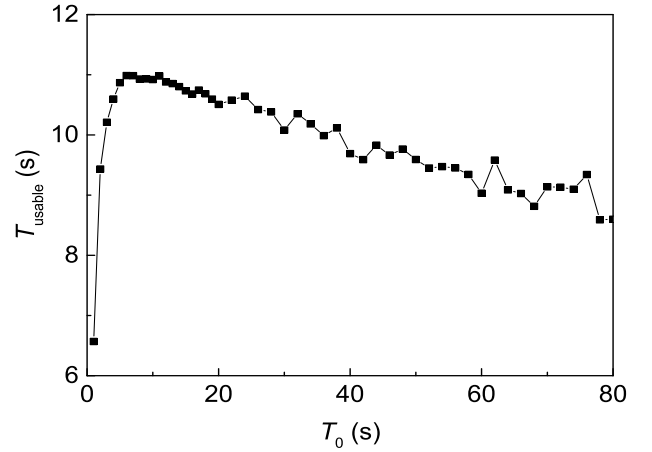


FIG. S10. Usable time  $T_{\text{usable}}$  until the phase deviation  $\Delta\phi_{\text{rms}}$  between predicted and actual phase for a single laser exceeds 1 rad calculated for different durations  $T_0$  of the preceding observation interval.

distribution of linewidths is intrinsic to  $1/f$  noise and not due to additional technical perturbations.

## COHERENCE TIME

The coherence time  $T_{\text{co}}$  can be defined [S16] as the time where the autocorrelation function  $R_E(\tau)$  has fallen to a certain fraction (e.g.  $1/2$  or  $1/e$ ) of its value at  $\tau = 0$ . According to Eq. (S5) the definition of coherence time  $T_{\text{co}}$  by  $R_E(T_{\text{co}}) = 1/e$  corresponds to  $\Delta\phi^2(T_{\text{co}}) = 2 \text{ rad}^2$ .

A relation between coherence time and FWHM linewidth  $\Delta\nu$  can be found in [S16] which gives  $T_{\text{co}} = 1/\Delta\nu$  for rectangular,  $T_{\text{co}} = 0.32/\Delta\nu$  for Lorentzian and  $T_{\text{coh}} = 0.66/\Delta\nu$  for Gaussian spectra.

### Coherence time for Ramsey interrogations

For Ramsey spectroscopy, the frequency of the interrogating laser needs to be measured in advance. Depending on the observation time  $T_0$  chosen to measure the frequency, the quality of the predicted phase evolution and thus the usable time  $T_{\text{usable}}$  until the phase deviation between predicted and actual phase for a single laser exceeds  $\Delta\phi_{\text{rms}} = 1 \text{ rad}$  may change. Using the measured phase data, we have calculated  $T_{\text{usable}}$  as a function of the preceding observation time (Fig. S10). The steep decrease of  $T_{\text{usable}}$  towards short observation times results from the increased influence of high frequency noise that leads to a poor predictability. The decrease at long observation times is a property of the  $1/f$  frequency noise. The optimal observation time  $T_0 \approx 4 \text{ s}$  leads to a  $T_{\text{usable}}$  of 11 s which is the practical coherence time for the application in two-pulse Ramsey interrogation of atoms.

## Coherence time for Rabi interrogations

For Rabi interrogation the frequency of the laser does not need to be known in advance but can be determined retrospectively from the result of the measurement. To cover the fluctuating average frequency during the Rabi interrogation, in analogy to the principle of a FFT spectrum analyzer, we consider an array of atomic ensembles at slightly differing center frequencies. Then the location of the maximum excitation probability provides information about the average frequency during the interrogation. In this scenario, a useful coherence time may be defined as the maximum time where the on-resonance excitation probability is not reduced too much from unity. If we linearize the optical Bloch equation, in analogy to the Strehl ratio in wave optics [S17] the maximum excitation probability is approximated by

$$P_{\max} = e^{-\langle \Delta\phi_{\text{rms}}^2 \rangle}. \quad (\text{S29})$$

We simulate this condition by dividing a 23 h phase evolution data interval in equal-length intervals of duration  $T_0$  which corresponds to the Rabi interrogation time. We obtain the average frequency in each interval by a least-squares fit to the phase data and subtract it from the measured phase evolution.

Fig. S11 shows the remaining phase  $\Delta\phi$  of the beat signal between Si2 and Si3 for an interval length of  $T_0 = 55$  s for 100 consecutive intervals. The accumulated rms phase  $\Delta\phi_{\text{rms}}(t)$  during each interval is shown in red. Note that due to fitting all these curves depend on the chosen interval length  $T_0$ . Because the spectrum of the phase fluctuation strongly increases towards low frequency, residual phase fluctuations after removing the fit contains a strong component with frequency  $1/2T_0$  which leads to the peculiar shape of  $\Delta\phi_{\text{rms}}(t)$ . To apply Eq. (S29) we have to take the rms value of the red curve within  $[0, T_0]$ . For the conditions of Fig. S11 we find for the beat  $\langle \Delta\phi_{\text{rms}}^2 \rangle = 1 \text{ rad}^2$ . Assuming identical laser performance the rms phase of each laser is then given by  $\Delta\phi_{\text{rms}}^2 = 1/2 \text{ rad}^2$  and  $P_{\max} = 0.6$  which would be still a useful excitation probability. Thus this interval length of  $T_0 = 55$  s can be considered as practically relevant coherence time for Rabi interrogation.

It is interesting why for Ramsey and Rabi interrogation of quantum systems with a highly stable laser governed by flicker noise the derived coherence time largely differs as 11 s and 55 s, respectively. One can understand this difference by the amount of prior information available for the interrogation. In Ramsey interrogation one has to estimate the mean frequency of the laser (and possibly its drift rate) from the previous evolution of these quantities. Flicker noise in the laser field inevitably means that the real phase evolution differs from the predicted one during the interrogation period. In Rabi interrogation, less prior information is needed since the measurement by itself

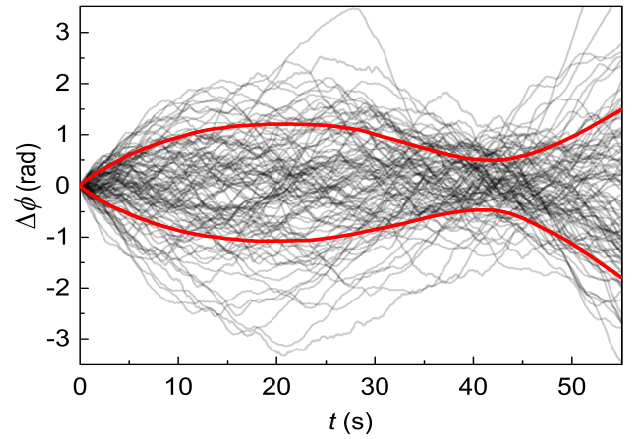


FIG. S11. Measured phase fluctuations of the beat of 100 consecutive curves (thin gray lines) with the phase from the average frequency  $\bar{\nu}$  over  $[0, T_0]$  with  $T_0 = 55$  s of each curve subtracted. The red lines indicate the  $\pm\Delta\phi_{\text{rms}}(t)$  range, calculated from 1500 curves. For this length of the temporal average of the rms fluctuations  $\langle \Delta\phi_{\text{rms}}^2 \rangle$  is 1 rad.

gives the actual information about the mean frequency. Here, the situation is pretty much the same as with the linewidth measurement with a spectrum analyzer. There any drift of the mean frequency will only lead to a shift of the acquired field spectrum. Thus both the information on the average frequency and the linewidth is available afterwards. In contrast, the Ramsey interrogation can only deliver information about this mean frequency as long as the phase difference between atomic coherence and laser field remains within  $\pm\pi$ , which puts much more severe constraints on the quality of the prediction.

## Relation between Allan deviation and coherence time

To predict the future phase under the condition of non-stationary frequency fluctuations, as in the case of flicker and random walk frequency noise, the future frequency needs to be estimated using an average frequency from the past values. As a convenient way for extrapolation over a duration  $T_0$  in an interval  $[t, t + T_0]$ , the average frequency from the preceding interval with the same duration  $[t - T_0, t]$  can be used. The variance between successive frequencies is used in the definition of the Allan deviation

$$\sigma_y^2(T_0) = \frac{1}{\nu_0^2} \left\langle \frac{1}{2} (\bar{\nu}_{i-1} - \bar{\nu}_i)^2 \right\rangle \quad (\text{S30})$$

$$= \frac{1}{4\pi^2 T_0^2 \nu_0^2} \left\langle \frac{1}{2} (\Delta\phi_{i-1} - \Delta\phi_i)^2 \right\rangle, \quad (\text{S31})$$

where  $\nu_0$  denotes the average frequency,  $\bar{\nu}_i$  the average frequency over the interval of duration  $T_0$ , and  $\langle \cdot \rangle$  the expectation value. If the frequency is adjusted to the

frequency of the preceding interval, this corresponds to  $\Delta\phi_{i-1} = 0$ , and thus

$$\Delta\phi_{\text{rms}}^2 = 8\pi^2\nu_0^2 T_0^2 \sigma_y^2(T_0) = \langle \Delta\phi_i^2 \rangle. \quad (\text{S32})$$

This equation allows to estimate the coherence time from the measured frequency stability as shown in Fig. 1. A phase deviation of  $\Delta\phi_{\text{rms}} = 1$  rad corresponds to an Allan deviation of

$$\sigma_y(T_0) = \frac{1}{2\sqrt{2}\pi\nu_0} T_0^{-1}. \quad (\text{S33})$$

The coherence time  $T_{\text{co}}$  is then defined by the intersection with the individual frequency stability of the lasers.

The Allan deviation plot (Fig. 1) shows that the coherence time for Si2 and Si3 is about 11 s. Please note that  $T_{\text{co}}$  is not limited by the short term stability of the lasers, but only by the flicker floor, given by the thermal noise of the cavities.

On the other hand, if the average frequency  $\bar{\nu}$  is determined from the measurement itself using  $\bar{\nu} = (\phi(t+T_0) - \phi(t))/2\pi T_0$ , the maximum phase excursion is expected at the midpoint of the interval  $t + T_0/2$  and its variance is given by

$$\Delta\phi_{\text{rms}}^2 = \left\langle \left( \phi(t + T_0/2) - \frac{\phi(t + T_0) + \phi(t)}{2} \right)^2 \right\rangle, \quad (\text{S34})$$

which is

$$\Delta\phi_{\text{rms}}^2 = 1/4 \cdot (2\pi T_0/2)^2 \langle (\bar{\nu}_i - \bar{\nu}_{i+1})^2 \rangle, \quad (\text{S35})$$

where  $\bar{\nu}_i$  and  $\bar{\nu}_{i+1}$  denote the average frequency over the intervals  $[t, t + T_0/2]$  and  $[t + T_0/2, t + T_0]$ .

This can be expressed by the Allan deviation as:

$$\Delta\phi_{\text{rms}}^2 = 1/2 \cdot \pi^2 T_0^2 \nu_0^2 \sigma_y^2(T_0/2). \quad (\text{S36})$$

In the case of flicker noise, the corresponding coherence time  $T_0$  is longer by a factor of 4 compared to the case where the average frequency is predicted from past values only (Eq. (S32)).

### Coherence time in radio astronomy

In radio astronomy the coherence time  $T_{\text{co}}$  of an oscillator with frequency  $\nu_0$  is commonly estimated from the standard Allan deviation  $\sigma_y$  [S18–S20]:

$$2\pi\nu_0 T_{\text{co}} \sigma_y(T_{\text{co}}) = 1. \quad (\text{S37})$$

According to Eq. (S32) this definition corresponds to  $\Delta\phi_{\text{rms}} = \sqrt{2}$  [S21].

From the measured flicker floor of mod  $\sigma_y = 4 \times 10^{-17}$  (corresponding to standard Allan deviation  $\sigma_y = 5 \times 10^{-17}$ ) we thus find a coherence time of about 16 s which

is larger by a factor of  $\sqrt{2}$  compared to the value defined by Eq. (S33).

- 
- [S1] T. Middelmann, A. Walkov, G. Bartl, and R. Schödel, *Phys. Rev. B* **92**, 174113 (2015).
  - [S2] D. G. Matei, T. Legero, C. Grebing, S. Häfner, C. Lisdat, R. Weyrich, W. Zhang, L. Sonderhouse, J. M. Robinson, F. Riehle, J. Ye, and U. Sterr, *J. Phys.: Conf. Ser.* **723**, 012031 (2016).
  - [S3] G. Rupschus, R. Niepraschk, K. Jousten, and M. Kühne, *J. Vacc. Sci. Tech. A* **12**, 1686 (1994).
  - [S4] C. Hagemann, C. Grebing, T. Kessler, S. Falke, N. Lemke, C. Lisdat, H. Schnatz, F. Riehle, and U. Sterr, *IEEE Trans. Instrum. Meas.* **62**, 1556 (2013).
  - [S5] D. W. Allan and J. Barnes, in *Proceedings of the 35<sup>th</sup> Ann. Freq. Control Symposium* (Electronic Industries Association, Ft. Monmouth, NJ 07703, 1981) pp. 470–475, for corrections see [S22].
  - [S6] E. Benkler, C. Lisdat, and U. Sterr, *Metrologia* **52**, 565 (2015).
  - [S7] E. Rubiola, *Rev. Sci. Instrum.* **76**, 054703 (2005).
  - [S8] S. T. Dawkins, J. J. McFerran, and A. N. Luiten, *IEEE Trans. Ultrason. Ferroelectr. Freq. Control* **54**, 918 (2007).
  - [S9] G. Kramer and W. Klische, in *Proceedings of the 18th European Frequency and Time Forum, Guildford, UK* (IET, London, UK, 2004) pp. 595–602.
  - [S10] D. W. Allan, *IEEE Trans. Instrum. Meas.* **IM-36**, 646 (1987).
  - [S11] G. M. Stephan, T. T. Tam, S. Blin, P. Besnard, and M. Tetu, *Phys. Rev. A* **71**, 043809 (2005).
  - [S12] M. Bishof, X. Zhang, M. J. Martin, and J. Ye, *Phys. Rev. Lett.* **111**, 093604 (2013).
  - [S13] F. J. Harris, *Proc. IEEE* **66**, 51 (1978).
  - [S14] N. Von Bandel, M. Myara, M. Sellahi, T. Souici, R. Dardailon, and P. Signoret, *Opt. Express* **24**, 27961 (2016).
  - [S15] D. A. Steck, *Quantum and Atom Optics* (available online at <http://steck.us/teaching> (Revision 0.11.6, 24 February 2017)).
  - [S16] B. E. A. Saleh and M. C. Teich, *Fundamentals of Photonics* (John Wiley & Sons, Inc., New York, New York, 1991).
  - [S17] V. N. Mahajan, *J. Opt. Soc. Am.* **72**, 1258 (1982).
  - [S18] W. Klemperer, *Proc. IEEE* **60**, 602 (1972).
  - [S19] A. E. E. Rogers and J. M. Moran, Jr., *IEEE Trans. Instrum. Meas.* **IM-30**, 283 (1981).
  - [S20] A. R. Thompson, J. M. Moran, and G. W. Swenson, *Interferometry and Synthesis in Radio Astronomy* (Wiley, New York, 2007).
  - [S21] The radio astronomical definition of coherence time might originate from a different, not commonly used definition of the Allan deviation without a factor of 1/2 leading to Eq. (S37) [S18, S19].
  - [S22] D. Sullivan, D. Allan, D. Howe, and F. Walls, *Characterization of Clocks and Oscillators*, NIST Tech. Note 1337 (NIST, U.S. Department of Commerce, National Institute of Standards and Technology, 1990) (online available at <http://tf.boulder.nist.gov/general/pdf/868.pdf>).